ISSN 1070-3632, Russian Journal of General Chemistry, 2024, Vol. 94, No. 1, pp. 154–160. © Pleiades Publishing, Ltd., 2024.

Synthesis, Structure, and Properties of Hexaferrites of the $BaFe_{12-x}Cr_xO_{19}$ System

V. E. Zhivulin[a], D. S. Afanasyev[b], N. A. Cherkasova[a], A. R. Zykova[a], S. A. Gudkova[a,c], and D. A. Vinnik[a,b,c,*]

[a] *South Ural State University, Chelyabinsk, 454080 Russia*
[b] *St. Petersburg University, St. Petersburg, 199034 Russia*
[c] *Moscow Institute of Physics and Technology, Dolgoprudny, Moscow oblast, 141701 Russia*
**e-mail: vinnikda@susu.ru*

Received October 20, 2023; revised January 31, 2024; accepted February 2, 2024

Abstract—The work presents the results of the synthesis and study of hexaferrite of barium, which is substituted with chromium within limits. The method of obtaining samples of the $BaFe_{12-x}Cr_xO_{19}$ system for a wide range of x from 0 to 4, with a step $x = 0.5$, has been worked out. It has been found that the optimal parameters of the synthesis mode are: temperature 1400°C and exposure time 5 h. The chemical composition was monitored using an energy dispersion analyzer. The phase composition was monitored by powder diffractometry. Lattice parameters for single-phase samples were calculated on the basis of obtained diffractograms. A monotonous change in the unit cell parameters was revealed, which was to be expected for isomorphic replacement of iron in the initial matrix with a magnetoplumbite structure. The temperature stability regions of the created samples were studied by differential scanning calorimetry. The influence of the degree of chromium substitution on the Curie temperature due to weakening of the inter-exchange interaction has been established.

Keywords: barium hexaferrite, magnetoplumbite, solid solutions, ceramics, solid–phase synthesis, $BaFe_{12-x}Cr_xO_{19}$

DOI: 10.1134/S1070363224010158

INTRODUCTION

The task of modern materials science is to create functional materials with specified properties that meet the requirements of the industry. To adjust and modify characteristics of materials for the tasks of specific applications, it is very common to use partial ion substitution of individual elements of the initial matrix.

Ferrites of various types and solid solutions based on them are a separate class of materials that are promising from the point of view of further research and are in demand by the industry today. Ferrites with a magnetoplumbite structure deserve special attention among this class of materials, due to their properties and crystalline structure. These materials have become widespread in various industries, such as energy and microelectronics; these materials are especially promising for microwave electronics [1–3]. Hexaferrites have the following physical properties: high coercive force and magnetic permeability, and most importantly, due to their crystalline structure, they have significant anisotropy of properties [3]. The presence of five nonequivalent iron positions in the crystal lattice makes it possible to vary the working characteristics over a wide range by partial substitution [4]. For this purpose, both isovalent and heterovalent substitution of titanium [2], aluminum [5], manganese [6], zinc [7], etc. for iron is used. The choice of the method for barium hexaferrite synthesis depends on the requirements for the shape, structure, and properties of the intended final product. Thus, to obtain monocrystalline barium hexaferrite, a method of spontaneous crystallization of solutions in an air atmosphere using a resistance furnace is used [10]. Sol-gel [11], co-deposition [12], and hydrothermal reactions [14] methods are used to obtain low-dimensional ferrites with a developed surface. Solid-phase synthesis is used as the most technologically advanced and potentially scalable method [13].

Barium hexaferrite is a promising functional material from the point of view of research, which is in demand by the industry. Its special physical properties are important:

Table 1. Elemental composition and experimentally calculated gross formulas of system $BaFe_{12-x}Cr_xO_{19}$ samples

No.	Element content, %				Formula
	Fe	Ba	Cr	O	
1	37.7	3.4	0.0	58.9	$BaFe_{12}O_{19}$
2	31.8	2.9	1.5	63.9	$BaFe_{11.5}Cr_{0.5}O_{19}$
3	34.0	3.3	3.1	59.6	$BaFe_{11.0}Cr_{1.0}O_{19}$
4	28.3	3.0	4.2	64.5	$BaFe_{10.4}Cr_{1.6}O_{19}$
5	28.6	3.2	5.8	62.4	$BaFe_{9.9}Cr_{2.1}O_{19}$
6	26.3	3.1	7.6	63.0	$BaFe_{9.3}Cr_{2.7}O_{19}$
7	26.0	3.2	9.1	61.7	$BaFe_{8.9}Cr_{3.1}O_{19}$
8	23.6	3.1	10.5	62.8	$BaFe_{8.3}Cr_{3.7}O_{19}$
9	22.8	3.2	12.2	61.8	$BaFe_{7.8}Cr_{4.2}O_{19}$

high coercive force, magnetic permeability, chemical stability, and others. This material and solid solutions based on it are important for electronics, including the microwave range.

Ion substitution is a rather common way for modifying the structure and varying working characteristics. With all the variety of results presented at the moment in the scientific literature, we have found no systematic studies on chromium-substituted barium hexaferrite.

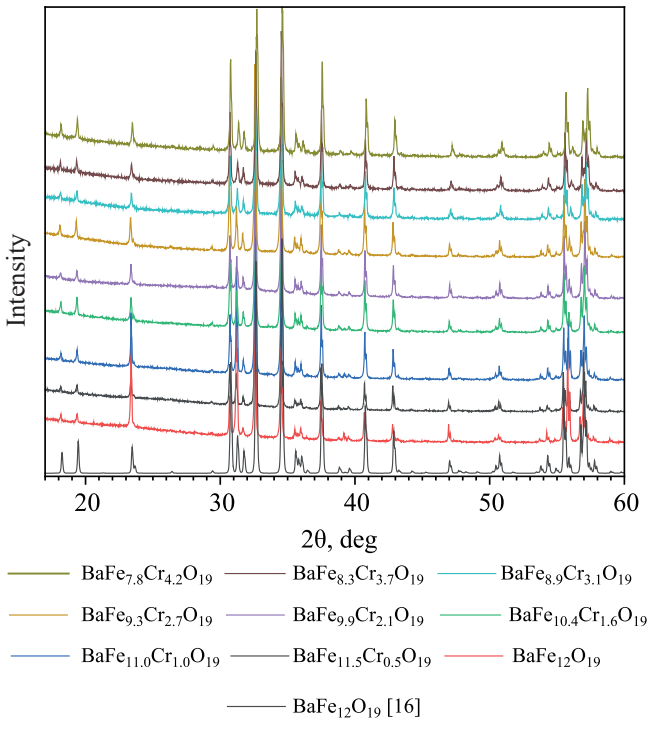

Fig. 1. X-ray diffraction patterns of the studied samples of the systems $BaFe_{12-x}Cr_xO_{19}$ and $BaFe_{12}O_{19}$ [16].

Based on fragmentary data on the effect of such isovalent substitution, as well as information about the ionic radius, electronic structure, and magnetic moment, the authors of this work considered this direction relevant.

In this work, a solid-phase synthesis method was used to study the effect of chromium substitution on the properties of the ceramics being created. This method provides a high yield of a suitable product, and also high reproducibility of experimental data, which is especially important for collecting statistics [15]. Similar studies in which barium hexaferrite was obtained by solid-phase synthesis also point to the effectiveness of this method.

RESULTS AND DISCUSSION

Table 1 shows the results of measuring the elemental composition according to energy dispersion spectroscopy data and the gross formulas calculated on its basis.

The X-ray images of the samples are shown in Fig. 1. The published data for unsubstituted barium hexaferrite $BaFe_{12}O_{19}$ [16] are also presented. It can be seen that all samples contain a single crystalline phase with the barium hexaferrite structure.

The parameters of the elementary crystal lattice were calculated from the X-ray patterns. Figure 2 shows the dependences of the change in the crystal lattice parameters *a, c* and *V* on the substitution degree *x*(Cr). It can be seen from Fig. 2 that an increase in the degree of iron substitution leads to a monotonous decrease in the crystal lattice parameters. The distortion of the crystal lattice occurs due to the fact that iron atoms with an ionic radius of Fe^{3+} (0.645 Å) are replaced by chromium atoms with a smaller ionic radius of Cr^{3+} (0.615 Å).

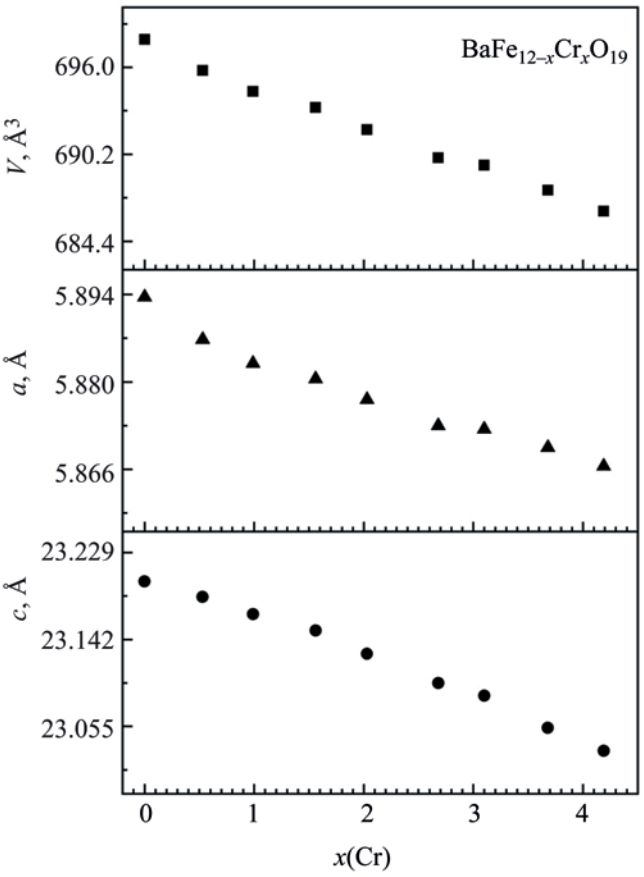

Fig. 2. Dependence of crystal lattice parameters *a, c* and volume *V* of $BaFe_{12-x}Cr_xO_{19}$ samples on the degree of chromium substitution *x*(Cr).

As a result of recrystallization of the chaotically arranged crystallites, micropores are formed. The nature of porosity is open. Figure 3 shows that in the mode of back-reflected electrons, no contrast associated with the atomic number of the element (atomic contrast) was detected; this fact is additional evidence in favor of the fact that the obtained samples are homogeneous and contain a single crystalline phase. The average grain size is 8 μm, and the average pore size is 4 μm.

The initial magnetic permeability was determined by measuring the inductance of a toroidal coil, the core of which was the ferrite under study.

Toroidal cores for measurements were prepared according to the following algorithm. The resulting ferrite ceramics were ground in an agate mortar. To improve pressing, 5 wt % of paraffin was added to the ferrite powder. The paraffin was dissolved in gasoline and the resulting solution was mixed with powder. After mixing and evaporation of the solvent, the resulting pressing mass was divided into granules of 0.5 mm in size.

Pressing was carried out in a composite mold, the upper and lower punsons in which had a hole. A rod was inserted into the hole to form the inner diameter of the ferrite ring. Pressing was carried out using a hydraulic press with a force of 0.5 tons. As a result of pressing, preforms with outer diameter 7 mm, inner diameter 3 mm, and height 5 mm were obtained.

The resulting preforms were placed on a platinum substrate and sintered. The furnace was heated in two stages. At the first stage, the temperature rose to 300°C with an isothermal exposure of 60 min. This step is necessary for burning out the binder paraffin. The second stage, heating to a temperature of 1400°C and isothermal exposure for 5 h, is necessary for sintering the powder.

After sintering, five coils of copper wire with a diameter of 0.2 mm and a length of 500 mm were wound onto each ferrite ring. The resulting coil was connected to an inductance meter. The inductance was measured at a frequency of 100 kHz. The value of the initial magnetic permeability was calculated using formula (1):

$$\mu = \frac{L2\pi}{\ln\left(\frac{R_1}{R_2}\right)hN^2\mu_0}, \quad (1)$$

where L is the inductance of the coil, R_1 is the outer diameter of the ring, R_2 is the inner diameter of the ring, h is the height of the ring, N is the number of turns of the wire, and μ_0 is the magnetic permeability of vacuum.

Table 2 shows calculated values of the initial magnetic permeability for the obtained ferrites. The

Table 2. Calculated values of initial magnetic permeability at a frequency of 100 kHz

No.	Sample formula	Initial magnetic permeability μ
1	$BaFe_{12}O_{19}$	18.4
2	$BaFe_{11.5}Cr_{0.5}O_{19}$	17.2
3	$BaFe_{11.0}Cr_{1.0}O_{19}$	14.5
4	$BaFe_{10.4}Cr_{1.6}O_{19}$	13.4
5	$BaFe_{9.9}Cr_{2.1}O_{19}$	13.4
6	$BaFe_{9.3}Cr_{2.7}O_{19}$	11.3
7	$BaFe_{8.9}Cr_{3.1}O_{19}$	13.5
8	$BaFe_{8.3}Cr_{3.7}O_{19}$	13.3
9	$BaFe_{7.8}Cr_{4.2}O_{19}$	19.5

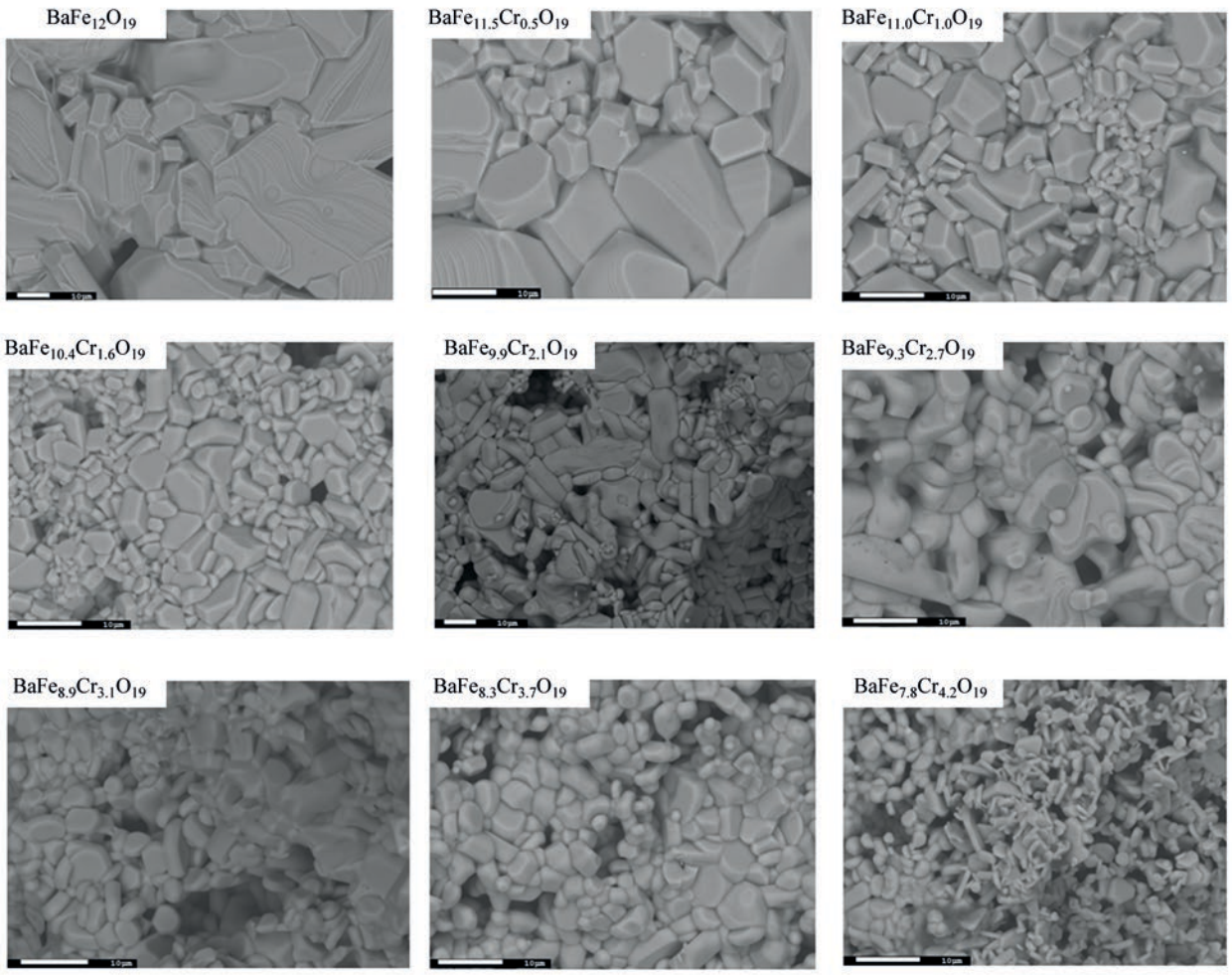

Fig. 3. Electronic images of the surface of ceramic samples $BaFe_{12-x}Cr_xO_{19}$ of various compositions, obtained in the back-reflected electron mode with magnification ×2000.

dependence of the initial magnetic permeability on the degree of substitution with chromium x(Cr), measured at a frequency of 100 kHz, is shown in Fig. 4 which shows that the magnetic permeability of ferrites changes nonmonotonically with an increase in the number of Cr atoms replacing iron. In the range of substitution degree from 0 to 2.7, a monotonous decrease in the magnetic permeability occurs. A further increase in the concentration of chromium atoms leads to an increase in the initial magnetic permeability.

The physical nature of the nonmonotonic behavior of the concentration dependence of magnetic permeability remains ambiguous and requires additional research.

The study of synthesized samples by differential scanning calorimetry (DSC) showed that samples with substitution degrees x(Cr) = 0–4 have an endothermic thermal effect. In this case, the heat capacity of the test sample changes. Cyclic measurements have shown that the temperature of this thermal effect is reproduced with high accuracy. The cooling cycle is accompanied by an exothermic effect at the same temperature and by a change in heat capacity. We associate this thermal effect with the ferromagnetic–paramagnetic phase transition (Curie temperature).

The DSC curves for all the studied samples were recorded under the same conditions. The weight of the suspension was 120 mg. The registration was performed in an argon current in the temperature range 30–600°C. Each of the studied samples was subjected to cyclic heating and cooling at three different rates of 10, 15, and

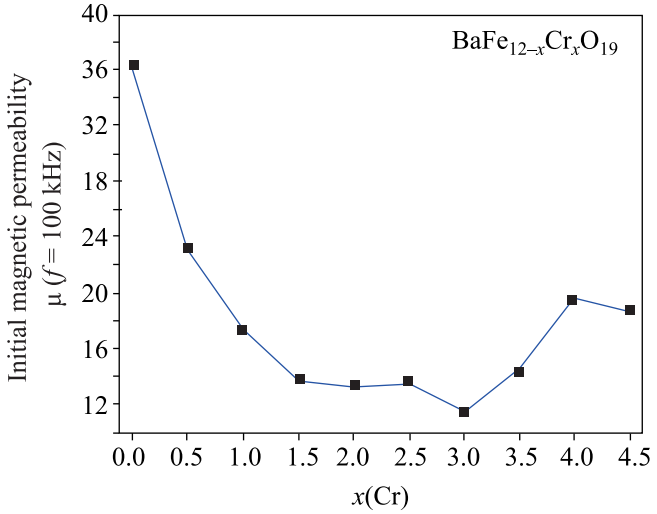

Fig. 4. Dependence of the initial magnetic permeability of ferrite at a frequency of 100 kHz on the substitution degree x(Cr) in the ferrite composition $BaFe_{12-x}Cr_xO_{19}$.

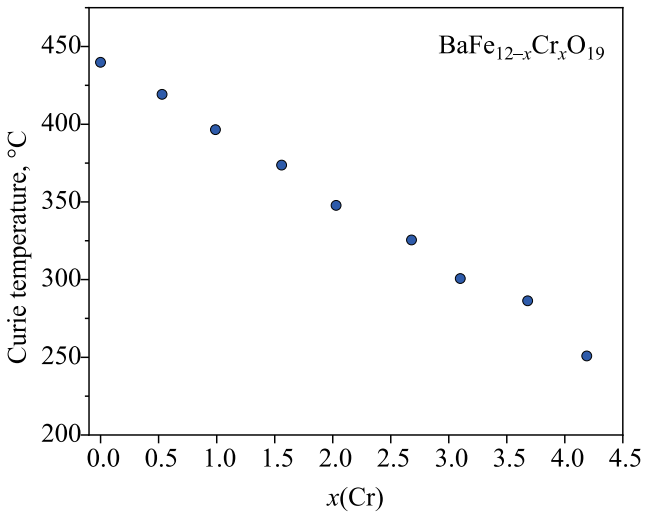

Fig. 5. Dependence of the Curie temperature on the degree of chromium substitution.

20 K/min. Due to the large mass of the test sample, the temperature of the maximum thermal effect depended on the measurement rate. To compensate for this, a linear approximation of the maximum value of the thermal effect at zero rate was performed. For this purpose, the maxima of thermal effects obtained at different heating rates were determined and their dependence on the heating rate was constructed. Next, the resulting line was approximated by a linear $y = b + kx$ function.

Figure 5 shows the temperature T_C change depending on the chromium content (x) for M-type hexaferrite $BaFe_{12-x}Cr_xO_{19}$. The T_C value of the initial crystal matrix $BaFe_{12}O_{19}$ coincides with the data [17]. As can be seen from Fig. 5, the temperature T_C decreases monotonously with an increase in the degree of chromium substitution for iron. The Cr(x) substitution reduces the over-exchange interaction between iron cations, which leads to a decrease in T_C.

CONCLUSIONS

Ferrite ceramics with a magnetoplumbite structure of the composition $BaFe_{12-x}Cr_xO_{19}$ (x varies from 0 to 4.2) were obtained by solid-phase synthesis. The physicochemical parameters of synthesis were worked out. It was shown that the optimal temperature for the solid-phase reaction is 1400°C. The isothermal exposure time is 5 h.

The study by X-ray diffraction analysis have shown that the replacement of Fe^{3+} ions with Cr^{3+} leads to a monotonous decrease in the parameters of the crystal lattice. It was revealed that as a result of the replacement of iron with chromium, the initial magnetic permeability changes non-monotonously. When replacing iron to the value x(Cr) = 2.7, the magnetic permeability decreases monotonously. Further substitution of iron to the value x(Cr) = 4.2 leads to an increase in magnetic permeability. The reason for the nonmonotonic change in the value of the initial magnetic permeability with monotonic replacement of iron ions by chromium ions remains unclear and requires additional research.

The study of the morphology of the obtained samples by scanning electron microscopy revealed the presence of open porosity of the resulting ceramics. It was also possible to qualitatively identify a decrease in the size of microcrystals with an increase in the degree of substitution with chromium.

The study by differential scanning calorimetry revealed the presence of a phase transition of the second kind, which is associated with the transition of the sample from a ferromagnetic state to a paramagnetic state (Curie temperature). An increase in the concentration of substituting chromium atoms leads to a decrease in the Curie temperature, which is caused by a decrease in the exchange interaction forces during the substitution of chromium for iron.

Table 3. Compositions of the initial mixture for the synthesis of system $BaFe_{12-x}Cr_xO_{19}$ samples

No.	Calculated formula	Composition, wt %		
		$BaCO_3$	Fe_2O_3	Cr_2O_3
1	$BaFe_{12}O_{19}$	17.079	82.921	0.000
2	$BaFe_{11.5}Cr_{0.5}O_{19}$	17.107	79.599	3.294
3	$BeFe_{11}Cr_1O_{19}$	17.136	76.265	6.599
4	$BaFe_{10.5}Cr_{1.5}O_{19}$	17.164	72.921	9.915
5	$BaFe_{10}Cr_2O_{19}$	17.193	69.565	13.242
6	$BaFe_{9.5}Cr_{2.5}O_{19}$	17.222	66.197	16.581
7	$BaFe_9Cr_3O_{19}$	17.251	62.819	19.930
8	$BaFe_{8.5}Cr_{3.5}O_{19}$	17.280	59.429	23.291
9	$BaFe_8Cr_4O_{19}$	17.309	56.028	26.663

EXPERIMENTAL

The studied samples were obtained by solid-phase synthesis. Iron oxide (Fe_2O_3), chromium oxide (Cr_2O_3), and barium carbonate were selected as the initial components of the charge; the concentrations of the starting substances are shown in Table 3. All reagents used are chemically pure. The components were mixed and ground in an agate mortar after calcination in a stoichiometric ratio. Then, tablets were prepared from the resulting mixtures using a metal mold and a hydraulic press. The diameter of the mold was 13 mm. The pressing force was 4 tons.

The tablet obtained as a result of pressing was heated in a muffle electric furnace. The temperature of sintering all samples was 1400°C. The duration of the isothermal exposure was 5 h. The morphological features of the surface and the elemental composition were studied using a JEOL model JSM7001F electron scanning microscope equipped with an INCAX-max 80 (Oxford Instruments) X-ray energy dispersion spectrometer. The phase composition and structure of the obtained samples were studied using a Rigaku powder diffractometer Optima IV model (CuK_α radiation).

FUNDING

This work was supported by St. Petersburg State University (grant no. 103751372).

CONFLICT OF INTEREST

The authors declare no conflict of interest.

REFERENCES

1. Khongorzul, B., Jargalan, N., Tsogbadrakh, N., Odkhuu, D., Trukhanov, S.V., Trukhanov, A.V., and Sangaa, D., *Ceram. Int*., 2023, vol. 49, p. 15492. https://doi.org/10.1016/j.ceramint.2023.01.134
2. Vinnik, D.A., Zhivulin, V.E., Uchaev, D.A., Gudkova, S.A., Zhivulin, D.E., Starikov, A.Yu., Trukhanov, S.V., Turchenko, V.A., Zubar, T.I., Gavrilova, T.P., Eremina, R.M., Fadeev, E., Lähderanta, E., Sombra, A.S.B., Zhou, D., Jotania, R.B., Singh, C., and Trukhanov, A.V., *J. Alloys Compd*., 2020, vol. 859. Article 158365. https://doi.org/10.1016/j.jallcom.2020.158365
3. Yustanti, E., Noviyanto, A., Chotimah, L.C., Saputra, M.A.R., Randa, M., and Manawan, M., *Coatings*, 2022, vol. 12, p. 1367. https://doi.org/10.3390/coatings12091367
4. Vinnik, D.A., Klygach, D.S., Chernukha, A.S., Zhivulin, V.E., Galimov, D.M., Starikov, A.Yu., Rezvy, A.V., Semenov, M.E., and Vakhitov, M.G., *Bull. SUSU Ser. Metallurgy*, 2017, vol. 17, no. 3, p. 28. https://doi.org/10.14529/met170304
5. Anantharamaiah, P.N., Shashanka, H.M., Saha, S., Haritha, K., and Ramana, C.V., *ACS Omega*, 2022, vol. 7, p. 6549. https://doi.org/10.1021/acsomega.2c04943
6. Al-Hammadi, A.H., Othman, A.A.M., and Khoreem, S.H., *Biointerface Res. Appl. Chem*., 2023, vol. 13, p. 369. https://doi.org/10.33263/BRIAC134.369
7. Verma, S., Chawla, A., Pushkarna, I., Singh, A., Godara, S.K., Pathak, D.K., Kumar, R., and Singh, M., *Mater. Today Commun*., 2021, vol. 27, p. 102291. https://doi.org/10.1016/j.mtcomm.2021.102291

8. Trukhanov, A.V., Kostishyn, V.G., Panina, L.V., Korovushkin, V.V., Turchenko, V.A., Thakur, P., Thakur, A., Yang, Y., Vinnik, D.A., Yakovenko, E.S., Macuy, L.Y., Trukhanova, E.L., and Trukhanov, S.V., *J. Alloys Compd*., 2018, vol. 754. https://doi.org/10.1016/j.jallcom.2018.04.150
9. Thang, P.D., Tiep, N.H., Ho, T.A., Nguyen, C., Nguyen, H., Dongquoc, V., Lee, B.W., Phan, T.L., Dang, N., Khan, D.T., and Yang, D.S., *J. Alloys Compd*., 2021, vol. 867, p. 158794. https://doi.org/10.1016/j.jallcom.2021.158794
10. Vinnik, D.A., Trofimov, E.A., Zhivulin, V.E., Zaitseva, O.V., Gudkova, S.A., Starikov, A.Yu., Zherebtsov, D.A., Kirsanova, A.A., Häßner, M., and Niewa, R., *Ceram. Int.*, 2019, vol. 45, p. 12942. https://doi.org/10.1016/j.ceramint.2019.03.221
11. Rattanaburi, P., Porrawatkul, P., Teppaya, N., Noypha, A., Pimsen, R., Chanthai, S., and Nuengmatcha, P., *Asian J. Chem*., 2022, vol. 34, p. 1113. https://doi.org/10.14233/ajchem.2022.23564
12. Singh, J., *Environ. Sci. Eng*., 2022, p. 833. https://doi.org/10.1007/978-3-030-96554-9_55
13. da Silva-Soares, P., da Costa-Catique, L., Guerrero, F., Mariño-Castellanos, P., Govea-Alcaide, E., Romaguera-Barcelay, Y., Rodrigues, A., Padrón-Hernández, E., and Peña-Garcia, R., *J. Magn. Magn. Mater*., 2022, vol. 547. https://doi.org/10.1016/j.jmmm.2021.168958
14. Guo, D., Zhou, P., Hou, J., Luo, X., Wang, X., and Deng, L., *IEEE Trans. Magn*., 2015, vol. 51. Article 2800804. https://doi.org/10.1109/TMAG.2015.2434884
15. Solidozoda, I.A., Zhivulin, V.E., Sherstyuk, D.P., Starikov, A.Yu., Trofimov, E.A., Zaitseva, O.V., and Vinnik, D.A., *Bull. SUSU Ser. Chem*., 2020, vol. 12, p. 110. https://doi.org/10.14529/chem200408
16. Townes, W.D., Fang, J.H., and Perrotta, A.J., *Z. Kristallogr*., 1967, vol. 125, p. 437. https://doi.org/10.1524/zkri.1967.125.125.437
17. Bezlepkin, A.A. and Kuntsevich, S., *Phys. Sol. State*, 2020, vol. 62, p. 1179. https://doi.org/10.1134/S1063783420070045